

ORIGINAL ARTICLE

Outer retinal thickness and visibility of the choriocapillaris in four distinct retinal regions imaged with spectral domain optical coherence tomography in dogs and cats

Elisa Mischi¹  | Petr Soukup¹  | Christine D. Harman² | Kazuya Oikawa³ | Malwina E. Kowalska^{1,4} | Sonja Hartnack⁴ | Gillian J. McLellan³ | András M. Komáromy²  | Simon A. Pot¹ 

¹Ophthalmology Section, Equine Department, Vetsuisse Faculty, University of Zurich, Zurich, Switzerland

²Department of Small Animal Clinical Sciences, College of Veterinary Medicine, Michigan State University, East Lansing, Michigan, USA

³Department of Ophthalmology and Visual Sciences, School of Medicine and Public Health, University of Wisconsin-Madison, Madison, Wisconsin, USA

⁴Section of Epidemiology, Vetsuisse Faculty, University of Zurich, Zurich, Switzerland

Correspondence

Simon A. Pot, Ophthalmology Section, Vetsuisse Faculty, University of Zurich, Winterthurerstrasse 260, Zurich 8057, Switzerland.
Email: spot@vetclinics.uzh.ch

Funding information

Core Grant for Vision Research, Grant/Award Number: P30 EY016665; National Institutes of Health (NIH), Grant/Award Number: P30 EY016665, R01 EY027396, R01EY025752 and S10 OD018221

Abstract

Purpose: To evaluate the outer retinal band thickness and choriocapillaris (CC) visibility in four distinct retinal regions in dogs and cats imaged with spectral domain optical coherence tomography (SD-OCT). To attempt delineation of a fovea-like region in canine and feline SD-OCT scans, aided by the identification of outer retinal thickness differences between retinal regions.

Methods: Spectralis® HRA + OCT SD-OCT scans from healthy, anesthetized dogs ($n = 10$) and cats ($n = 12$) were analyzed. Scanlines on which the CC was identifiable were counted and CC visibility was scored. Outer nuclear layer (ONL) thickness and the distances from external limiting membrane (ELM) to retinal pigment epithelium/Bruch's membrane complex (RPE/BM) and ELM to CC were measured in the area centralis (AC), a visually identified fovea-like region, and in regions superior and inferior to the optic nerve head (ONH). Measurements were analyzed using a multilevel regression.

Results: The CC was visible in over 90% of scanlines from dogs and cats. The ONL was consistently thinnest in the fovea-like region. The outer retina (ELM-RPE and ELM-CC) was thickest within the AC compared with superior and inferior to the ONH in dogs and cats ($p < .001$ for all comparisons).

Conclusions: The CC appears a valid, albeit less than ideal outer retinal boundary marker in tapetal species. The AC can be objectively differentiated from the surrounding retina on SD-OCT images of dogs and cats; a fovea-like region was identified in dogs and its presence was suggested in cats. These findings allow targeted imaging and image evaluation of these regions of retinal specialization.

KEYWORDS

area centralis, cat, choriocapillaris, dog, outer retina, SD-OCT

[Correction added on 08 July 2022, after first online publication: CSAL funding statement has been added.]

This is an open access article under the terms of the [Creative Commons Attribution-NonCommercial-NoDerivs](https://creativecommons.org/licenses/by-nc-nd/4.0/) License, which permits use and distribution in any medium, provided the original work is properly cited, the use is non-commercial and no modifications or adaptations are made.

© 2022 The Authors. *Veterinary Ophthalmology* published by Wiley Periodicals LLC on behalf of American College of Veterinary Ophthalmologists.

1 | INTRODUCTION

Spectral domain optical coherence tomography (SD-OCT) is a non-invasive, noncontact, light-wave based imaging technique for cross-sectional imaging studies of the ocular fundus and the anterior segment of the eye. SD-OCT is especially useful for in vivo imaging of the retina and optic nerve head (ONH) in research and clinical settings.^{1–10}

The use and utility of SD-OCT have been advocated for primary glaucoma, sudden acquired retinal degeneration syndrome (SARDS), retinal dysplasia (RD), and progressive retinal atrophy (PRA) in veterinary patients.^{11–21} Evaluation of retinal layer integrity and accurate measurement of thicknesses of and distances between anatomic layers require consistent and reliable identification of these anatomic layers on SD-OCT scans. Moreover, correct identification of the outer retinal boundary is vital for proper segmentation of retinal layers on OCT images across species, and thus for reproducibility and translation of clinical examination and research results.²² Finally, a uniform nomenclature of SD-OCT anatomy is indispensable when comparing studies to avoid discrepancies regarding the interpretation of SD-OCT findings.²²

The inner retinal layers that are recognizable on human SD-OCT scans have undisputed histological correlates, but the histological correlates of the outer retinal bands on human SD-OCT scans have not been so readily established.^{23–28} Nevertheless, a consensus statement on nomenclature for the outer retinal bands distinguishable on human SD-OCT scans has been agreed upon and published by Staurengi et al.²⁹ Here, the panel specialists agreed that the retinal pigment epithelium/Bruch's membrane complex (RPE/BM) can consistently be identified as the outermost continuous hyperreflective band on human SD-OCT scans.²⁹ De Ramus et al.³⁰ presented a uniform standard for murine OCT layer nomenclature, in which they identified the choroid as an intensely hyperreflective band directly external to the RPE/BM. Detailed images of outer retinal layer anatomy visible on canine^{1,10,17,21,31–34} and feline^{16,35} SD-OCT scans have been published. Unfortunately, a consensus nomenclature of the outer retinal bands distinguishable on SD-OCT scans, similar to that in humans²⁹ and mice,³⁰ has not been established in other species.

As mentioned above, the outermost intensely hyperreflective band visible on human SD-OCT scans represents the RPE/BM, which can thus be used as a reliable outer retinal boundary marker in humans.^{22,24,29} However, Soukup et al. demonstrated that choroidal structures can have similar or higher reflectivity than the RPE/BM on SD-OCT images of minipigs, rabbits, rats, and mice,²² consistent with previous observations in mice.³⁰ This can lead to difficulties in the consistent identification of the RPE/

BM and thus, renders the RPE/BM unreliable as an outer retinal boundary in these species.²² Indeed, especially on SD-OCT scans from species with a tapetum lucidum, a specialized inner choroidal structure that reflects light back toward and through the retina,³⁶ the RPE/BM can be difficult to separate from the intense tapetal reflectivity in the inner choroid (see Figure S1).^{16,31} This has led to inconsistent interpretations in the literature of what layer represents the RPE/BM on SD-OCT scans of dogs.^{1,31}

In both tapetal and non-tapetal species, the first structure external to the RPE/BM is the choriocapillaris (CC), which shares a common basement membrane (Bruch's membrane) with the RPE. Small vessels which do not cross the RPE/BM connect the CC with the more externally located major choroidal vessels.^{22,36–38} Soukup et al.²² demonstrated that both the CC and connecting vasculature are visible on SD-OCT scans and are valid markers for the identification of the outer retinal boundary, that are readily distinguished in minipigs, rabbits, rats and mice, which are all non-tapetal species. Personal observations based on our own SD-OCT library led us to hypothesize that, despite the intense tapetal reflectivity, the CC can also reliably be identified as an outer retinal boundary marker in tapetal species like dogs and cats.

Dogs and cats possess an *area centralis* (AC), which is a region of retinal specialization with a high photoreceptor cell density located superotemporal to the ONH. The AC is located within the visual streak, has a horizontally elongated oval form and is largely devoid of retinal vessels.^{15,16,31,37,39,40} Beltran et al.³¹ first described a primate-fovea-like bouquet of cone photoreceptors within the AC of the canine retina. This fovea-like region was characterized by a thinning of the ONL visible on SD-OCT and an elongation of cone outer segments visible on histology.³¹ Thinning of the ONL in the AC and elongation of photoreceptor inner and outer segments in the center of the AC was subsequently confirmed by Occelli et al.¹⁰ on canine SD-OCT scans. Pathologies located in these regions of retinal specialization, as in human patients with macular diseases,⁴¹ can be expected to have a greater impact on canine and feline vision than more peripherally located lesions. However, the impact of focal retinal changes on visual behavior in dogs and cats has not been evaluated to date, possibly as a result of a lack of readily available, objective measures to assess structure–function relationships in patients with focal retinal pathology. SD-OCT examination data provide high resolution information regarding structural integrity of the retina and are thus a valuable clinical and experimental endpoint, especially if SD-OCT would allow targeted evaluation of regions of retinal specialization. A case in point is the study by Iwabe et al.⁴² With the use of SD-OCT, histopathology, and an obstacle-avoidance course, the authors demonstrated that

small islands of preserved retina within the AC result in preserved visual behavioral function, despite severe retinal damage in RHO mutant dogs following light exposure.⁴² Furthermore, reliable identification of a fovea-like region may position dogs and cats as attractive model species for retinal disease research, particularly pertinent to the human macula.^{16,31,39}

Based on the personal observations in our own SD-OCT image library, we hypothesize that a fovea-like region can be visually identified within the canine and feline AC, and that significant differences in the thickness of the ONL (as described in dogs by Beltran et al.³¹) and photoreceptor layers (as identified in 12-week-old dogs by Occelli et al.¹⁰) can inform objective distinction of the AC and fovea-like regions from the surrounding retina on SD-OCT scans of adult canine and feline retinas.

The purpose of this study is two-fold: (1) To evaluate the reliability of the CC as an identifiable marker for the outer retinal boundary on SD-OCT scans from tapetal species; and (2) to attempt delineation of a fovea-like region within the canine and feline AC by SD-OCT, aided by the identification of differences in outer retinal thickness between retinal regions in the datasets available for this study.

2 | MATERIALS AND METHODS


2.1 | Animals

Spectral domain optical coherence tomography B-scans of untreated control animals enrolled in various clinical and translational studies were retrieved from image databases at the Komáromy laboratory, Department of Small Animal Clinical Sciences, College of Veterinary Medicine, Michigan State University, MI, USA, and the McLellan laboratory, Department of Ophthalmology and Visual Sciences, School of Medicine and Public Health, University of Wisconsin-Madison, WI, USA. All animal studies, during which these images were acquired, were approved by Institutional Animal Care and Use Committees of the Michigan State University and the University of Wisconsin-Madison, respectively, and were conducted in compliance with the ARVO Statement on the Use of Animals in Ophthalmic and Vision Research.

Spectral domain optical coherence tomography B-scans were obtained from 10 healthy Beagle dogs, group-housed in the same environment at the Michigan State University College of Veterinary Medicine (Table 1). The dogs were genotyped for the G661R *ADAMTS10* missense mutation as previously described.⁴³

Spectral domain optical coherence tomography B-scans were also obtained from 12 healthy adult domestic

TABLE 1 Signalment of dogs included in the study

	Breed	Gender	Age [months]	Genetic status
1	Beagle	M	6.6	Carrier
2	Beagle	F	71.2	Carrier
3	Beagle	F	6.6	Carrier
4	Beagle	M	42.1	Carrier
5	Beagle	F	17.6	wt
6	Beagle	F	9.8	wt
7	Beagle	F	9.7	wt
8	Beagle	M	9.2	wt
9	Beagle	F	41.1	wt
10	Beagle	F	41.9	wt

Note: Breed, gender, age at time point of SD-OCT-imaging (median age of 13.7 months) and the genetic status are listed for all 10 dogs; Carrier = unaffected carrier for G661R *ADAMTS10* open-angle glaucoma mutation, wt = wild type, M = male, F = female.

short hair cats, housed in a laboratory animal facility at the University of Wisconsin-Madison for the purposes of other long-term, non-invasive pre-clinical studies (electrophysiology and ocular imaging) (Table 2). The cats were genotyped for the *LTBP2* mutation as previously described.²⁰


All animals underwent a complete ocular examination (intraocular pressure evaluation via rebound tonometry, slit lamp biomicroscopy, fluorescein staining, indirect ophthalmoscopy) to rule out the presence of ocular diseases prior to inclusion in this study.

2.2 | Image acquisition and analysis

All images were acquired with a Spectralis® HRA + OCT combined confocal scanning laser ophthalmoscopy (cSLO) and SD-OCT system (Heidelberg Engineering) equipped with a 30° noncontact lens (Heidelberg Engineering). All imaging was performed with the animals under general anesthesia, using routine and approved protocols. Since the data evaluated in this study were retrieved from existing databases of two different laboratories, the OCT scan acquisition protocols varied between dogs and cats.

Dogs were premedicated with IV acepromazine maleate (0.02 mg/kg, Butler Schein Animal Health) and then induced with IV propofol (4 mg/kg or to effect, Propoflo™28, Abbott Laboratories). Anesthesia was maintained with isoflurane (Akorn Inc.). The anesthesia protocol used in cats included IM Ketamine (12.5–25 mg/kg, VetaKet®, Akorn Inc.) and IM Xylazine (0.5–1 mg/kg, AnaSed®, Akorn Inc.). The pupils were dilated with 1% tropicamide (Akorn, Inc.) prior to or at induction of anesthesia. In dogs, the eyes were kept

TABLE 2 Signalment of cats included in the study

	Breed	Gender	Age [months]	Genetic status
1	Domestic short hair	F	67.3	wt
2	Domestic short hair	F	11.9	Carrier
3	Domestic short hair	F	6.5	Carrier
4	Domestic short hair	M	11.7	Carrier
5	Domestic short hair	F	11.7	Carrier
6	Domestic short hair	M	11.6	Carrier
7	Domestic short hair	M	11.7	Carrier
8	Domestic short hair	M	11.7	Carrier
9	Domestic short hair	M	25.0	Carrier
10	Domestic short hair	M	25.0	Carrier
11	Domestic short hair	M	25.5	Carrier
12	Domestic short hair	M	24.4	wt

Note: Breed, gender, age at time point of SD-OCT-imaging (median age of 11.8 months) and the genetic status are listed for all 12 cats; Carrier = unaffected obligate heterozygous carrier for a mutation in *LTP2* causal for recessively inherited feline primary congenital glaucoma, wt = wild type, F = female, M = male.

lubricated with repeated application of BSS sterile irrigating solution (Alcon®, Alcon Laboratories) during anesthesia. The globes were immobilized with conjunctival stay sutures (4–0 silk; Ethicon Inc.) and kept open with the help of a wire eyelid speculum, if needed. In cats, custom rigid gas permeable plano contact lenses were applied (Soderberg Optical Inc.), following application of 1% proparacaine (Proparacaine Hydrochloride Ophthalmic Solution, USP 0.5%, Bausch & Lomb Inc.)

and artificial tears (Refresh Tears®, Allergan, Inc.) and a wire eyelid speculum was placed. No stay sutures were used for cats, since the use of ketamine ensured a central eye position.

Canine SD-OCT B-scans that were analyzed included 200 averaged line scans (produced by processing 9–17 raw B-scans into a single averaged B-scan) selected from 28 scan volumes. Line scans from one volume centered over the ONH (130 line scans) and one volume that included the ONH and the AC in the region superotemporal to the ONH (70 line scans) were included for image analysis (Figure 1). Feline SD-OCT B-scans that were analyzed included 46 highly averaged single line scans (produced by processing 93–100 raw B-scans into a single highly averaged B-scan) from areas superior and inferior to the ONH. Moreover, 176 averaged line scans (produced by processing 7–11 raw B-scans into a single averaged B-scan) selected from 22 scan volumes that included the ONH and the AC in the region superotemporal to the ONH were included for image analysis (Figure 1).

B-scans for which the Spectralis® system-specific internal quality value (signal-to-noise-ratio in decibels) was less than 20 dB, and B-scans that were acquired by averaging less than seven individual B-scans, were excluded from the study.

All image analyses were performed by two independent graders (EM, PS) using HEYEX software (Heidelberg Eye Explorer, Version 1.10.2.0, Heidelberg Engineering) in four different retinal regions: one superior (dorsal) to the optic nerve head (dONH), representing the tapetal area, one inferior (ventral) to the ONH (vONH), representing the non-tapetal area, and one in a visually identified AC and fovea-like region (F). The mean distances from the center of the ONH to dONH and vONH regions were 2.8 mm (range: 2.5–4.1 mm) and 1.7 mm (range: 1.3–2.3 mm) for dogs and cats, respectively. The AC was visually identified on cSLO images as an area superotemporal to the ONH surrounded by centripetally arranged retinal vessels (Figure 2). Five single scan lines passing through the visually identified AC were selected from the scan volumes centered over the region superotemporal to the ONH for analysis of the AC and F.

The fovea-like region (F) was visually identified on SD-OCT images of the avascular center of the AC if the following features were observed: thinning of the ONL and NFL and thickening of the photoreceptor outer segment layers (with the ELM and ellipsoid zone (EZ) arching internally (Figure 2). The AC and fovea-like region were visually identified by consensus opinion from three observers (EM, PS, and SAP) given the subjective nature of this identification. The reviewer panel consisted of one experienced OCT scan reader (PS), one inexperienced (student) OCT scan reader (EM), who was trained by PS and

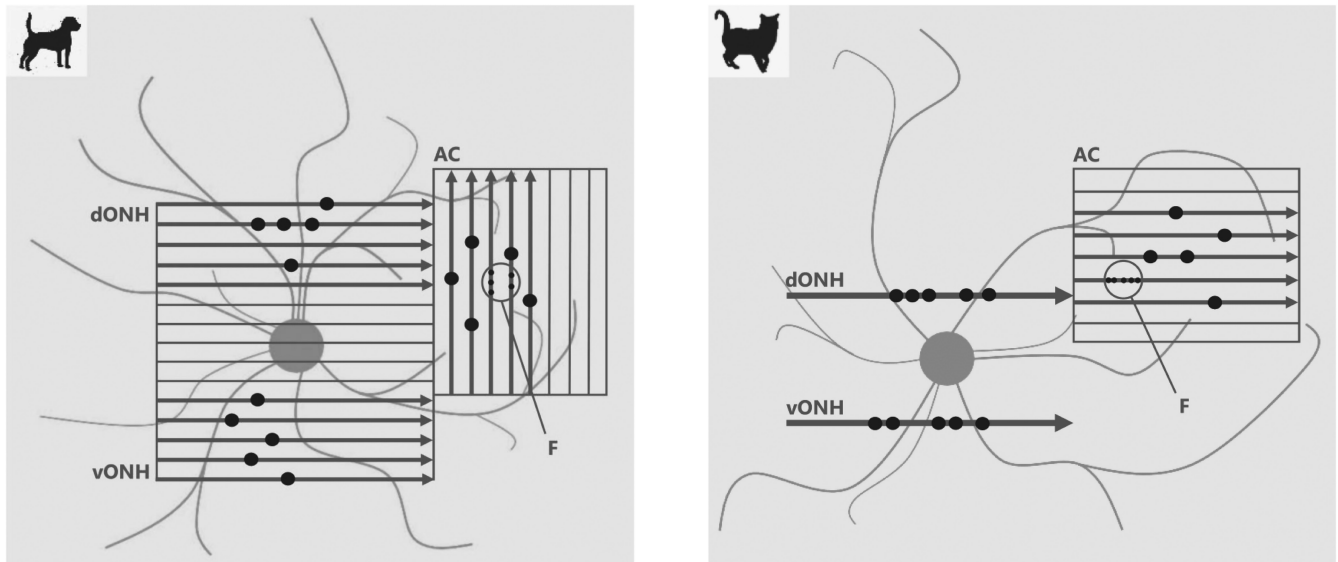


FIGURE 1 SD-OCT scan orientation and line scan and measurement point selection. Left: Schematic of the canine fundus with available SD-OCT volume scans. Right: Schematic of the feline fundus with available SD-OCT highly averaged line scans and volume scan. The four retinal regions that were evaluated are superior (dorsal) to the optic nerve head (dONH), inferior (ventral) to the ONH (vONH), and in a visually identified area centralis (AC) and fovea-like region (F). The five top and bottom single scan lines (arrows) were selected from the volume scans centered over the ONH for analysis of the dONH and vONH regions in dogs. The highly averaged line scans located dorsal and ventral to the optic nerve head (arrows marked dONH and vONH) were selected for analysis of the dONH and vONH regions in cats. Five single scan lines (arrows) passing through the visually identified AC were selected from the scan volumes centered over the region superotemporal to the ONH for analysis of the AC and F. The arrows represent the scan direction. The dots mark the single randomly selected measurement positions. Measurements in the dONH, vONH, and AC were limited to the central 50% of the B-scan image width to avoid possible image distortion artifacts at the edges of the scans. In the fovea-like region (circles marked 'F'), five measurement points were randomly selected within a radius of 100 μm from the perceived center of the fovea-like region. Note, the fovea-like region is not drawn to scale but enlarged approximately tenfold for illustrative purposes

gained experience during the project, and one experienced veterinary ophthalmologist (SAP).

2.2.1 | Qualitative analysis: Choriocapillaris (CC) identifiability and visibility

To evaluate the visibility of the CC, the innermost narrow hyporeflective horizontal choroidal band visible on SD-OCT images was identified on all available scan lines of dogs (200) and cats (222) in the regions dONH, vONH, and AC. Connection of this presumed CC through narrow hyporeflective canals (connecting vasculature) to the more externally located major choroidal vessels was ascertained on these and adjoining SD-OCT B-scans (Figure 3). First, the question whether the CC could be identified at all was answered by both graders with a yes/no answer. Second, CC visibility was estimated by both graders as a percentage of SD-OCT B-scan length with visible CC. The visibility of the CC was evaluated based on a scoring system with three scores:

- Score 1: CC visible on less than 10% of the image width.
- Score 2: CC visible on 11%–50% of the image width.

Score 3: CC visible on more than 50% of the image width.

2.2.2 | Quantitative analysis: Outer retinal band thickness

Three different layer measurements were manually performed on SD-OCT images to support the identification of the CC and of a fovea-like region within the canine and feline AC (Figure 2). The first measurement represented the combined length of photoreceptor inner and outer segments and was defined as the linear distance between ELM and the border between the interdigitation zone (IZ) of the photoreceptor outer segment tips with the apical processes of the RPE and the RPE, not including the RPE/BM complex (ELM-RPE). The second measurement represented the outer retinal thickness and was defined as the linear distance between ELM and the CC, including the RPE/BM complex (ELM-CC). The numerical difference between the first and second measurements yielded the thickness of the RPE/BM complex on SD-OCT. The ONL was included as third measurement and

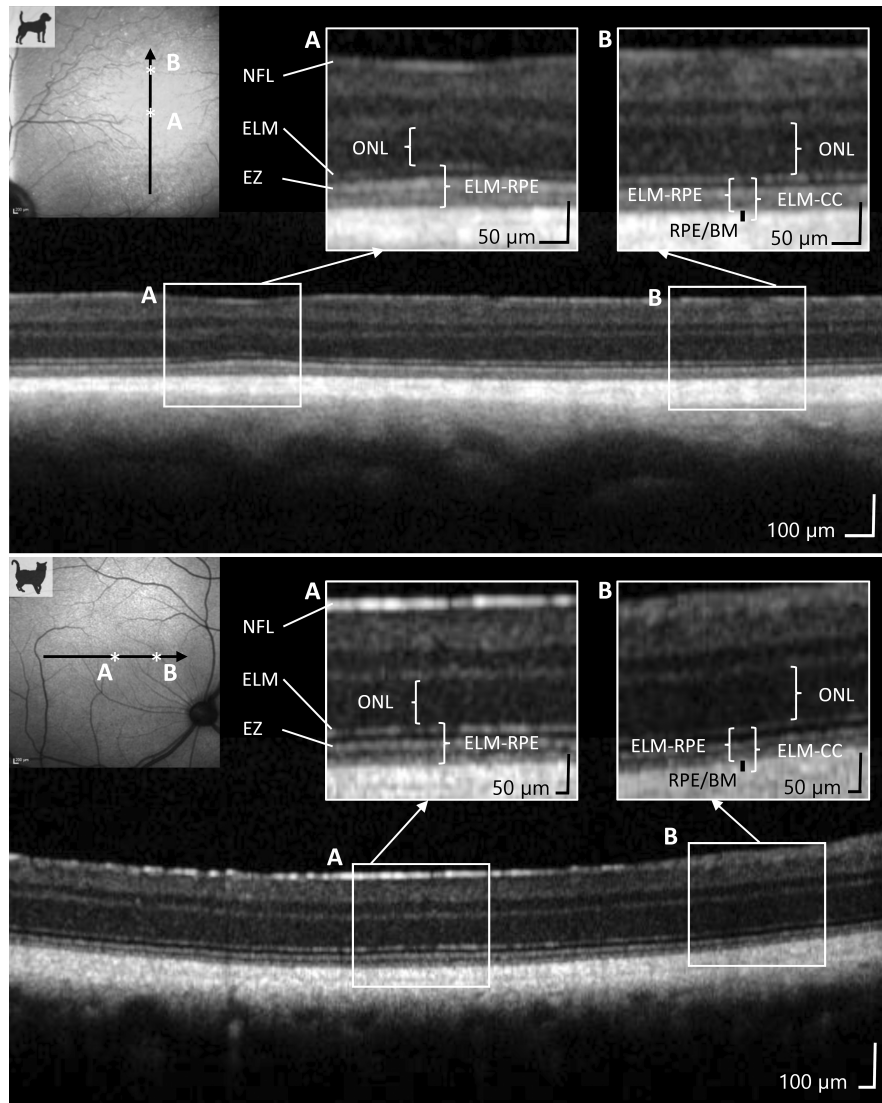


FIGURE 2 Identification of the area centralis (AC) and the fovea-like region (F). Top left in top panel: cSLO image of canine retina OS; top left in bottom panel: cSLO image of feline retina OD. Next to the cSLO images: SD-OCT B-scan through the center of the AC in the same dog and cat, respectively. The AC was visually identified on the cSLO image as area dorsotemporal to the ONH, surrounded by centripetally arranged retinal vessels. The F was visually identified on SD-OCT images of the avascular center of the AC (asterisk A), through observation of the following features: thinning of the ONL and internal arching of the ELM and EZ (left cut-out A). Measurement of outer retinal band thicknesses. Three different measurements were performed: 1. ELM-RPE, 2. ELM-CC, 3. ONL. The numerical difference between first and second measurement = thickness of the RPE/BM complex. Measurements of ONL and ELM-RPE in the F are illustrated in the left cut-outs (A). Note that the ONL is thinner and the ELM-RPE distance is larger in the F compared to the surrounding AC, illustrated in the right cut-outs (B, corresponding to asterisk B). CC, choriocapillaris; ELM, external limiting membrane; EZ, ellipsoid zone; NFL, nerve fiber layer; ONL, outer nuclear layer; RPE/BM, retinal pigment epithelium/Bruch's membrane

used as internal quality control for correct visual identification of the fovea-like region as previously described by Beltran et al.³¹

Measurements of ELM-RPE, ELM-CC, and ONL each were performed in five randomly selected measurement points per previously defined retinal region: dONH, vONH, AC, and F. Measurements in the dONH, vONH, and AC regions were limited to the central 50% of the B-scan image width to avoid possible image distortion artifacts at the edges of the scans. In the fovea-like region,

five measurement points were randomly selected within a radius of 100 μm from the perceived center of the fovea-like region (Figure 1). All measurements were performed in micrometers.

2.3 | Statistical evaluation

Multilevel regression analysis was used to assess the effects of retinal region (dONH, vONH, and AC), grader,

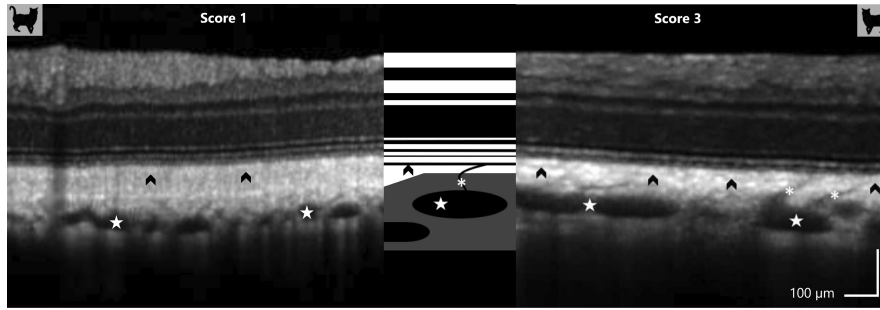


FIGURE 3 Visibility of the choriocapillaris (CC) on feline SD-OCT B-scan images. Left: Score 1 SD-OCT B-scan image of the dONH region of a cat (Score 1: CC visible on <10% of the image width). Middle: Schematic of the different hyperreflective and hyporeflective retinal and choroidal bands visible on SD-OCT B-scans of tapetal species. Right: Score 3 SD-OCT B-scan image of the AC region of a cat (Score 3: CC visible on >50% of the image width). The black arrowheads represent the CC, which is visible as the innermost narrow hyporeflective horizontal choroidal band throughout almost the entire image width on the score 3 scan. Note that the CC is more difficult to visualize on the score 1 scan in the left image. Also note that the tapetum is thicker on the scan that received a visibility score 1 than on the scan that received a score 3. The white asterisks represent small blood vessels that cross the tapetum to connect the CC to the more externally located major choroidal vasculature (white stars). Identification of these narrow hyporeflective connecting vessels was used to ascertain correct identification of the CC. AC, area centralis; dONH, retinal region superior (dorsal) to the optic nerve head

eye (OD = *oculus dexter* [right eye], OS = *oculus sinister* [left eye]), and replication (five repeat measurements) on the mean retinal layer measurements. Since a fovea-like region could only be identified on the SD-OCT images of five canine and five feline eyes, F was excluded from statistical analyses other than descriptive analyses. The low number of measurements for F compared with dONH, vONH, and AC caused an imbalance in factorial level, which is undesired in parametric linear models. A separate model was built for each retinal layer (ELM-RPE, ELM-CC, and ONL). Animal number was included in all models as a random effect to adjust for replication. Variables for the final models were selected based on the Akaike Information Criterion (AIC) and likelihood ratio test. In addition, we performed a multiple post hoc comparison (Tukey multiple comparisons test) between retinal regions in each retinal layer.

Statistical analyses were performed with IBM SPSS Statistics Version 25 and R version 3.5.2, using the packages multcomp and nlme.

The null hypothesis stated that the measurement means are equal across retinal regions. The null hypothesis was rejected at $p < .05$.

The qualitative CC identifiability (Yes/No) and visibility (scoring) analyses of grader A and grader B were compared via Cohen's Kappa coefficient calculation with agreement classification according to Kundel and Polansky⁴⁴ and Landis and Koch.⁴⁵ Only the averaged SD-OCT B-scans extracted from the scan volumes from the dogs and cats which had a comparable image quality were included in this interrater agreement analysis. The interrater agreement analysis for the highly averaged single line scans from the cats was performed separately.

3 | RESULTS

Figure 4 illustrates our interpretation and terminology for the retinal bands seen on SD-OCT images used in this work.

The CC could be identified as a thin hyporeflective horizontal linear structure external and adjacent to the hyperreflective horizontal RPE/BM on SD-OCT images.

3.1 | Qualitative results: Choriocapillaris (CC) identifiability and visibility

The interrater agreement results of the Cohen's Kappa test for CC identifiability and visibility scoring for both dogs and cats are presented in Table 3.

The interrater agreement for CC identifiability and visibility scoring in dogs was "fair." Grader A identified the CC on 182, and grader B on 163 of 200 B-scans, with disagreement between graders on 15.5% of the B-scans. The graders disagreed regarding CC visibility scoring on 27.5% of the B-scans. Most canine B-scans (Grader A: 145/200, Grader B: 150/200) received score 1 (CC visible on <10% of the image width; Figure S2) and no canine B-scans received score 3 (CC visible on >50% of the image width) from either grader, independent of retinal region.

The interrater agreement for CC identifiability and visibility scoring on averaged scans in cats was "substantial." Grader A identified the CC on 160, and grader B on 161 of 176 averaged B-scans, with disagreement between graders on <5% of the B-scans. The graders disagreed regarding CC visibility scoring on 11.5% of the averaged B-scans. The interrater agreement for CC identifiability and visibility scoring

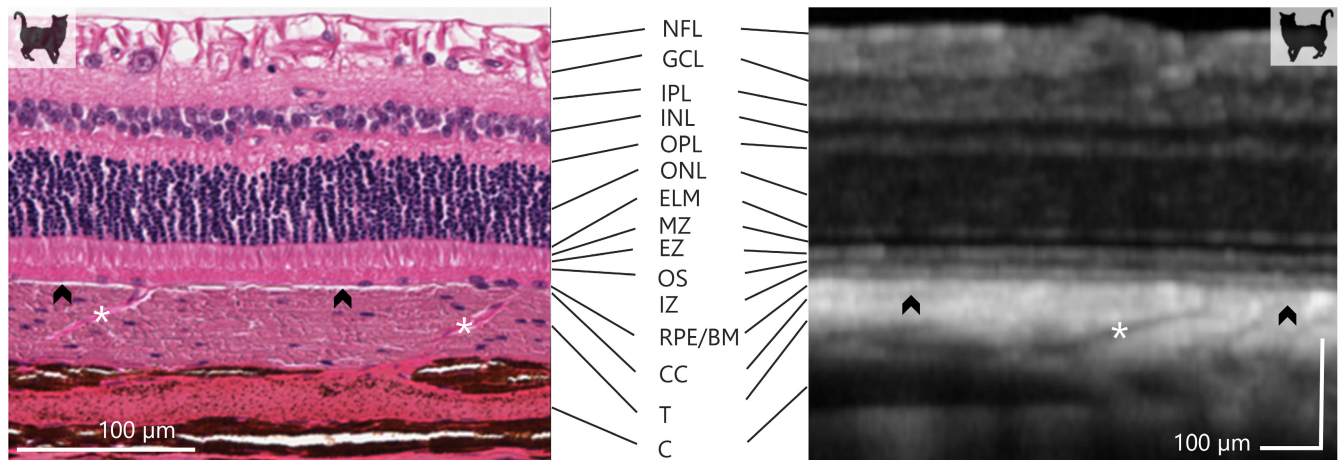


FIGURE 4 Juxtaposition of SD-OCT with retinal histology. The hyporeflective and hyperreflective retinal bands of the feline retina and choroid visible on SD-OCT B-scans (right image) juxtaposed and compared to histology (left image). The nomenclature of the different retinal layers/zones was based on the SD-OCT nomenclature consensus published by Staurenghi et al.²⁹ C, choroid; CC, choriocapillaris; ELM, external limiting membrane; EZ, ellipsoid zone; GCL, ganglion cell layer; INL, inner nuclear layer; IPL, inner plexiform layer; IZ, interdigitation zone; MZ, myoid zone; NFL, nerve fiber layer; ONL, outer nuclear layer; OPL, outer plexiform layer; OS, outer segments; RPE/BM, retinal pigment epithelium/Bruch's membrane; T, tapetum. White asterisks indicate the small vessels connecting the CC with the more externally located major choroidal vasculature. The black arrowheads indicate the CC

TABLE 3 Interrater agreement of choriocapillaris (CC) identifiability and visibility in dogs and cats

SD-OCT B-scan type	CC identifiability (Yes/No)		CC visibility (scoring)	
Averaged	K-value = 0.36	Fair	K-value = 0.29	Fair
Averaged	K-value = 0.75	Substantial	K-value = 0.72	Substantial
Highly averaged	K-value = 1	Almost perfect	K-value = 0.71	Substantial

Note: Two hundred canine and 176 feline averaged SD-OCT B-scans were used to assess CC identifiability, where both graders answered with yes or no whether the CC could be identified at all; and CC visibility, where both graders scored the percentage of SD-OCT B-scan length with a visible CC. A Cohen's Kappa test was used to test interrater agreement. The last line in the table represents the interrater agreement for an additional 46 highly averaged single line scans of cats, which were analyzed separately. Averaged line scans were produced by processing 9–17 and 7–11 raw B-scans into a single averaged B-scan in dogs and cats, respectively. Highly averaged single line scans of cats were produced by processing 93–100 raw B-scans into a single highly averaged B-scan. Kappa results were interpreted as follows: <0 = poor, 0–0.20 = slight, 0.21–0.4 = fair, 0.41–0.60 = moderate, 0.61–0.80 = substantial, 0.81–1.00 = almost perfect.⁴⁵

on highly averaged scans in cats was “perfect” and “substantial,” respectively. Both graders identified the CC on all 46 highly averaged (from 93–100 raw B-scans) single line scans. The graders disagreed regarding CC visibility scoring on 13% of the highly averaged B-scans. Most averaged feline B-scans (Grader A: 143/176, Grader B 122/176) received score 1 (CC visible on <10% of the image width), whereas most highly averaged feline B-scans (Grader A: 32/46, Grader B: 34/46) received score 2 (CC visible on 10%–50% of the image width) from both graders. Averaged feline B-scans received score 3 (CC visible on >50% of the image width) once, and highly averaged feline B-scans received score 3 three times from both graders (see Figure 3 for example).

All scoring disagreements between grader A and B consisted of a one grade difference in scoring.

Scan reflectivity profiles were generated to demonstrate differences between visibility scores 1 and 3 in felines and between scores 1 and 2 in canines (Figure 5).

3.2 | Qualitative results: Visual identification of the fovea-like region

A fovea-like region (F) was visually identified in five eyes of four dogs on SD-OCT images of the avascular center of the AC from 14 scan volumes, including the ONH and the

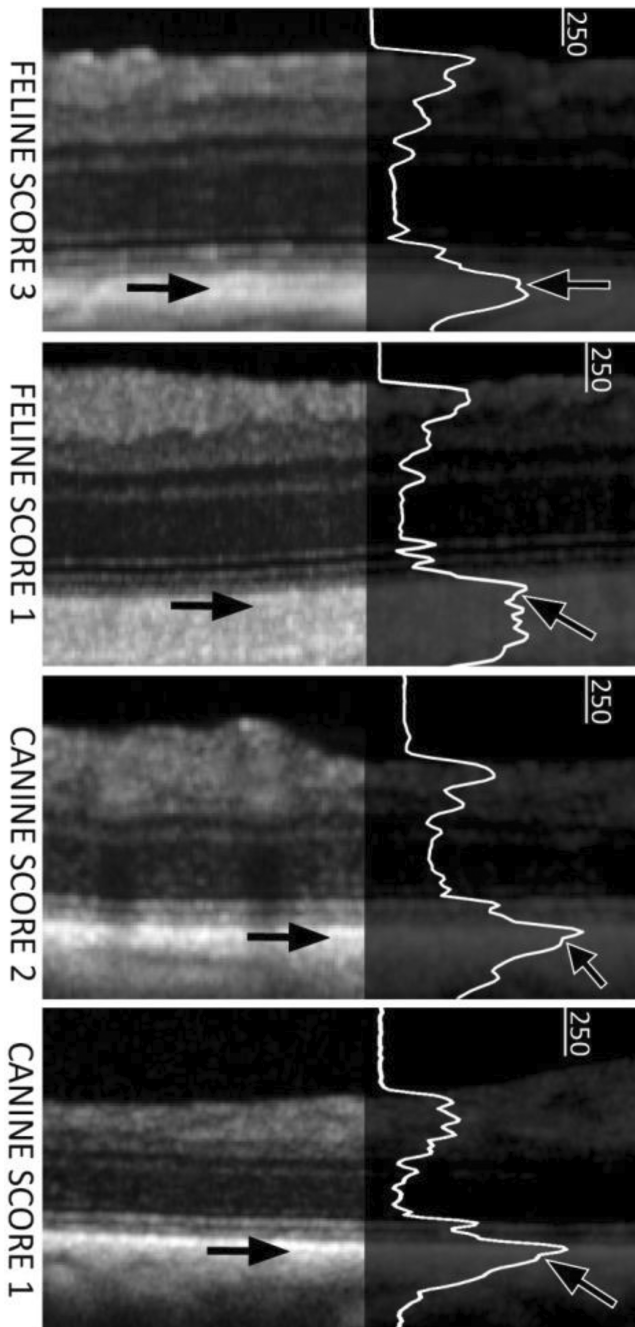


FIGURE 5 Reflectivity profile images of canine and feline SD-OCT scans. Left: SD-OCT scans of highest and lowest score regarding CC visibility in cats and dogs. Right: Reflectivity profile images generated from these SD-OCT scans. Score 1 = CC visible on <10% of the image width. Score 2 = CC visible on 11%–50% of the image width. Score 3 = CC visible on >50% of the image width. Black arrows mark the CC. Reflectivity profiles were generated using Image J function ‘Analyze>Plot profile’ in scale of 256 shades of gray from 10 consecutive A-scans. CC, choriocapillaris

AC. A fovea-like region (F) was visually identified in five eyes of four cats on SD-OCT images of the avascular center of the AC from 20 scan volumes, including the ONH and

the AC (Figure S3). The anatomic lack of a foveal pit observed on human retinal SD-OCT scans has been termed fovea plana.⁴⁶ As illustrated in Figure 2 and S3, a fovea-like area with a partial fovea plana-like appearance was observed on the canine OCT scans, whereas a fovea-like area with a fovea plana-like appearance was observed on the feline OCT scans. Mean distance from the ONH center to the center of the AC (6.7 mm in dogs, 4.2 mm in cats) was comparable with the mean distance from the ONH center to the center of the F (6.2 mm in dogs, 4.2 mm in cats; Table S1). These results increased the authors' confidence in the correct visual localization of the avascular center of the AC and the fovea-like region.

3.3 | Quantitative results: Outer retinal band thickness

Measurements in μm of the combined length of photoreceptor inner and outer segments (ELM-RPE), the outer retinal thickness (ELM-CC) and the outer nuclear layer thickness (ONL) across four distinct retinal regions (F, AC, dONH, and vONH) on SD-OCT images of dogs and cats are compiled in Figure 6. The means and standard deviations of the retinal layer measurements are listed in Tables S2a,b.

The ELM-RPE and ELM-CC were thickest in the F, then AC, then dONH regions, and were thinnest in the vONH region, demonstrating very similar patterns in dogs and cats. The ONL on the other hand was thinnest in the F, then vONH, then AC regions and was thickest in the dONH region, again demonstrating a similar pattern in dogs and cats. Figure 2 illustrates the thinner ONL and thicker ELM-RPE measurements within the fovea-like region compared to the surrounding retina. The fact that the indirectly measured thickness of the RPE/BM was consistent and constant across all four retinal regions (mean: 10.2 μm in dogs, 10.1 μm in cats) increased the authors' confidence in the correct identification and localization of the CC in these eyes.

External limiting membrane-RPE, ELM-CC, and ONL thickness measurements were all statistically significantly different between AC, dONH, and vONH (see Tables S3a,b). Grader, eye (OD vs. OS), and replication did not affect the measurement means, apart from a statistically significant but unexplained grader effect on the ELM-RPE measurements in dogs. The estimated mean difference of this grader effect on the ELM-RPE measurements in dogs was 0.54 μm ($p = .004$, 95% CI from 0.2 to 0.9 μm) which constitutes a 1.2% difference between graders on a mean ELM-RPE thickness of 45.5 μm in dogs.

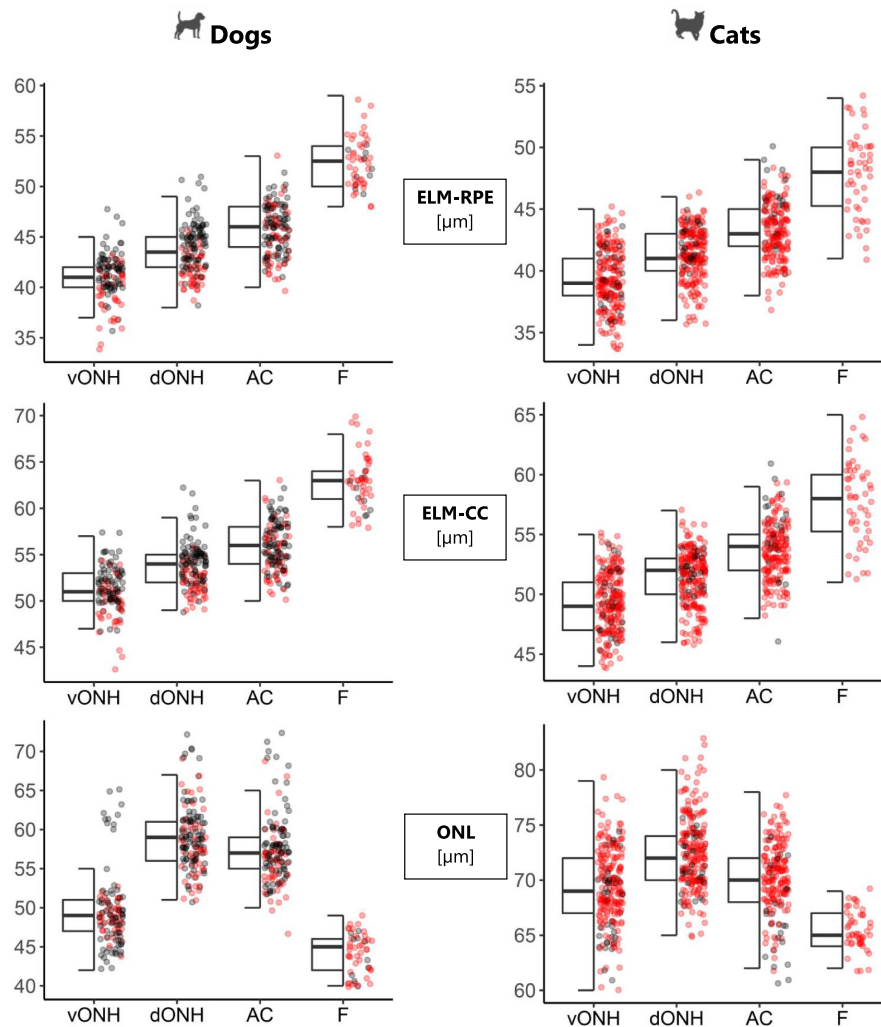


FIGURE 6 Retinal layer thickness measurements on SD-OCT B-scans in four distinct retinal regions in dogs and cats. Measurements of the combined photoreceptor inner and outer segment length (ELM-RPE), the outer retinal thickness (ELM-CC) and the outer nuclear layer thickness (ONL) on SD-OCT images of dogs (left side) and cats (right side) are presented. Boxplots with median, first quartile $Q_{0.25}$, third quartile $Q_{0.75}$ and statistical minimum and maximum (without outliers), and scatterplots with dots representing single measurements are depicted. For wildtype animals black dots are used and carriers are presented in red (dogs = heterozygous carriers for the G661R *ADAMTS10* mutation, cats = heterozygous carriers for the *LTBP2* mutation). Numbers on the y-axis represent thickness measurements in μm (ELM-RPE, ELM-CC, ONL). The four distinct retinal regions are indicated on the x-axis, from left to right: ventral to the ONH (vONH), dorsal to the ONH (dONH), area centralis (AC) and fovea-like region (F). CC, choriocapillaris; ELM, external limiting membrane; RPE, retinal pigment epithelium

4 | DISCUSSION

Interspecies variations in retinal and choroidal anatomy prevent a direct extrapolation of the human retinal SD-OCT-nomenclature to animals. The validation of markers used to identify retinal and choroidal structures on SD-OCT scans in different species is necessary. In the field of veterinary medicine, there are only relatively few and incomplete published datasets of normative SD-OCT-values for the different retinal and choroidal layers.^{1,10,12,17,21,22,33,47}

The reflective nature of the tapetum lucidum makes the RPE/BM difficult to identify and an unreliable outer

retinal marker, as in non-tapetal animal species where the choroidal structures have similar or higher reflectivity than the RPE/BM.²² The results of the study presented here supported our hypothesis that both the CC and connecting vasculature can be visualized on SD-OCT scans and might be useful as markers for the identification of the outer retinal boundary in dogs and cats, which are both tapetal species.³⁶

The value of the CC and its connecting vasculature as markers for the identification of the outer retinal margin in dogs and cats depends on their identifiability on individual B-scans. The CC was identifiable on a higher percentage of averaged line scans from dogs (>80% and

>90%, depending on the grader), and cats (>90%), than previously described for rabbits, rats and mice by Soukup et al.²² The CC is therefore a valid marker for the outer retinal boundary in dogs and cats. However, the fact that the CC was visible on <10% of the SD-OCT image in the majority of canine and feline scans and that interrater agreement in dogs was only fair suggests that visibility can be inconsistent, necessitating rigorous, and detailed scrutiny of the entire length of these scans. The tapetum lucidum with its reflectivity seemed to make the CC more difficult to visualize (Figures 3 and 5, and S2), compared to non-tapetal species in which visualization of the CC and its connecting vasculature was described as easy.²² The CC may thus be a less than ideal outer retinal margin marker for use in tapetal species, especially in situations where large numbers of scans need to be evaluated.

The CC was identified on all highly averaged line scans from cats by both graders, and the CC visibility scores were higher for highly averaged line scans compared with averaged line scans from cats. Disagreement between graders regarding specific scores was almost equal compared with the averaged scans. This means that the identifiability and visibility of the CC on SD-OCT B-scans would likely be increased by increasing the number of raw single B-scans acquired and averaged to produce a single averaged B-scan. The acquisition and evaluation of consecutive serial or volume B-scans could also increase CC identifiability and thus increase its usefulness as outer retinal margin marker, as previously suggested by Soukup et al.²²

Choriocapillaris identifiability and visibility scores were comparable for dogs and cats, but the interrater agreement for these scores was higher for cats than dogs. Differences in grader experience could have accounted for differences in scoring. With only a one grade difference in scoring for all scoring disagreements between graders A and B, the differences in scoring were relatively small overall, especially when the difference in experience level between the two graders is considered. The reasons for the difference in interrater agreement between cats and dogs are unclear.

A fovea-like region was visually identified in a subset of dogs (five eyes, four dogs) and cats (five eyes, four cats; Figure S3). This finding is in accordance with the description of a canine fovea-like region by Beltran et al.³¹ and the indication of the same by Occelli et al.,¹⁰ and suggests the potential existence of a similar fovea-like region in the AC in cats.

The distance between two scanlines in the B-scan volumes including the AC that were analyzed for the study presented here was 123 μm in dogs and 213 μm in cats. Therefore, the scanline density would explain the lack of

identification of a fovea-like region in a significant number of eyes in cats. However, due to the almost twofold higher scanline density, a higher rate of identification of a fovea-like region would have been expected in dogs compared to cats. The lack of a substantial difference in fovea-like region identification between dogs (5/14 scan volumes) and cats (5/20 scan volumes) despite the difference in scanline densities in our study might be explained by the presence of a larger fovea-like region in cats with more evenly thickened photoreceptor outer segment layers and/or thinned ONL, facilitating identification. Since published information on the existence or morphology of a fovea-like region in the retina of cats is lacking, and the study presented here lacks histopathologic evidence to substantiate the presence of a feline fovea-like region, further studies will be necessary in order to either support or reject this hypothesis. Of note, the authors believe that *ex vivo* histology, with all the induced post-mortem processing tissue changes and artifacts, and the necessity for very laborious serial sectioning within a consistent plane, is not an ideal gold standard technique for identification of a fovea-like region. This is especially true if layer thicknesses and structure differences within and outside of such a small fovea-like region are subtle. With these shortcomings, we question whether histology would be more sensitive at identifying a fovea-like region than *in vivo* OCT image evaluation.

In the current study, only visible anatomic markers on SD-OCT scans were used for the identification of the fovea-like region, including thinning of the ONL and NFL and thickening of the photoreceptor outer segment layer accentuated by internal arching of the ELM and EZ. The histology of the canine fovea-like region as presented by Beltran et al.³¹ demonstrates a significant, focal, increased thickness of the photoreceptor outer segment layer, much confined to the central 50% of its 200 μm diameter. The identification of these visible markers can therefore be expected to only be reliable in the center of the fovea-like region in dogs. The fact that volume scan segmentation, as described by Beltran et al.,³¹ resulted in a reliable identification of the fovea-like region using ONL thinning as an objective marker supports this claim. Manual segmentation of SD-OCT volume scans is possible,^{14,31,48} but very time-consuming and not a logistically feasible technique for the evaluation of clinical patients. For this reason, algorithms were developed for the automatic segmentation and analysis of SD-OCT datasets from human and rodent retinas acquired in clinical and research settings.^{2,49–59} Few algorithms, none of which are commercially available, are currently capable of segmenting canine retinal layers.^{60,61} Further development and use of such automated analysis techniques for

canine retinal SD-OCT scan evaluation is desirable for clinical and research work alike.

The fact that our ONH-AC and ONH-F distance measurements were basically identical (Table S1) strengthened the author's confidence in the correct visual localization of the avascular center of the AC and F in our study. This confidence was further supported by the comparable localization of the center of the AC on cSLO images in our study and those from Beltran et al.,³¹ Mowat et al.,¹⁵ and Occelli et al.¹⁰ Furthermore, various histopathology-based publications^{40,62,63} also placed the canine AC at a very similar location, despite potential processing artifacts and differences in measurement methods.

As demonstrated in our study, photoreceptor inner and outer segment length (ELM-RPE) and outer retina (ELM-CC) were significantly thicker inside compared with outside the AC, and thicker still, albeit not statistically evaluated, within the fovea-like region. These measurements therefore qualify as potential objective markers for the identification of the AC and fovea-like region, in addition to ONL thickness. This conclusion is supported by a recent publication which reported a demonstrable lengthening of photoreceptor inner/outer segments on SD-OCT scan images from the AC of dogs between 4 and 52 weeks of age, with an apparent peak inner/outer segment length in the very center of the AC demonstrated in 12-week-old dogs.¹⁰ These OCT-based observations are supported by the increased thickness of the photoreceptor outer segment layer that was previously demonstrated histologically by Mowat et al.³⁹ in the AC, and by Beltran et al.³¹ in the fovea-like region. There are no published or unpublished data from extensive studies in these research colonies, to date, that suggest any ocular pathology in either cats that are heterozygous for the *LTBP2* mutation or dogs that are heterozygous for the G661R *ADAMTS10* mutation. However, the potential difference in ELM-RPE and ELM-CC measurements in the vONH and dONH regions between wildtype and G661R *ADAMTS10* heterozygous carrier dogs (Figure 6) is an observation that would be worth pursuing further in a follow-up study including larger animal cohorts.

In conclusion, the CC and connecting vasculature are identifiable and appear to represent valid outer retinal boundary markers. However, the CC could only be visualized with close scrutiny of the entire scan length in most evaluated scans, making the CC a less than ideal outer retinal boundary marker for use in tapetal species. Moreover, the AC and a fovea-like region can be visually and objectively differentiated from the surrounding retina on canine SD-OCT scans and similar features suggestive of a fovea-like region were also observed in feline SD-OCT scans. The potential existence of a fovea-like region in the AC in cats was suggested.

ACKNOWLEDGMENTS

We thank Julie A Kiland and Carol A Rasmussen at the University of Wisconsin-Madison and Kristin Koehl and the Michigan State University Campus Animal Resources for their technical assistance. This work was supported by the NIH (R01EY025752 to AMK, R01 EY027396 and S10 OD018221 to GJM and Core Grant for Vision Research P30 EY016665 to the University of Wisconsin-Madison), by an unrestricted award from Research to Prevent Blindness to the Department of Ophthalmology and Visual Sciences, University of Wisconsin-Madison, and by a Japanese Student Services Organization (JASSO) scholarship to KO. CSAL statement was provided by Universitat Zurich.


CONFLICT OF INTEREST

The authors declare no conflict of interest.

ORCID

Elisa Mischi  <https://orcid.org/0000-0002-2852-897X>

Petr Soukup  <https://orcid.org/0000-0001-6125-8580>

András M. Komáromy  <https://orcid.org/0000-0002-8845-0588>

Simon A. Pot  <https://orcid.org/0000-0002-8782-7144>

REFERENCES

- Hernandez-Merino E, Kecova H, Jacobson SJ, Hamouche KN, Nzokwe RN, Grozdanic SD. Spectral domain optical coherence tomography (SD-OCT) assessment of the healthy female canine retina and optic nerve. *Vet Ophthalmol.* 2011;14:400-405.
- Garcia Garrido M, Beck SC, Muhlfridel R, et al. Towards a quantitative OCT image analysis. *PLoS One.* 2014;9:e100080.
- Huang D, Swanson EA, Lin CP, et al. Optical coherence tomography. *Science.* 1991;254:1178-1181.
- McLellan GJ, Rasmussen CA. Optical coherence tomography for the evaluation of retinal and optic nerve morphology in animal subjects: practical considerations. *Vet Ophthalmol.* 1991;15(Suppl 2):13-28.
- Sakata LM, Deleon-Ortega J, Sakata V, et al. Optical coherence tomography of the retina and optic nerve - a review. *Clin Experiment Ophthalmol.* 2009;37:90-99.
- Berger A, Cavallero S, Dominguez E, et al. Spectral-domain optical coherence tomography of the rodent eye: highlighting layers of the outer retina using signal averaging and comparison with histology. *PLoS One.* 2014;9:e96494.
- Fujimoto J, Swanson E. The development, commercialization, and impact of optical coherence tomography. *Invest Ophthalmol Vis Sci.* 2016;57:OCT1-OCT13.
- Thomas D, Duguid G. Optical coherence tomography--a review of the principles and contemporary uses in retinal investigation. *Eye (Lond).* 2004;18:561-570.
- Adhi M, Duker JS. Optical coherence tomography--current and future applications. *Curr Opin Ophthalmol.* 2013;24:213-221.
- Occelli LM, Pasmanter N, Ayoub EE, Petersen-Jones SM. Changes in retinal layer thickness with maturation in the dog: an in vivo spectral domain - optical coherence tomography imaging study. *BMC Vet Res.* 2020;16:225.

11. Young WM, Oh A, Williams JG, et al. Clinical therapeutic efficacy of mycophenolate mofetil in the treatment of SARDS in dogs—a prospective open-label pilot study. *Vet Ophthalmol.* 2018;21:565-576.
12. Grozdanic SD, Lazic T, Kecova H, Mohan K, Kuehn MH. Optical coherence tomography and molecular analysis of sudden acquired retinal degeneration syndrome (SARDS) eyes suggests the immune-mediated nature of retinal damage. *Vet Ophthalmol.* 2019;22:305-327.
13. Oh A, Foster ML, Williams JG, et al. Diagnostic utility of clinical and laboratory test parameters for differentiating between sudden acquired retinal degeneration syndrome and pituitary-dependent hyperadrenocorticism in dogs. *Vet Ophthalmol.* 2019;22:842-858.
14. Iwabe S, Dufour VL, Guzman JM, et al. Focal/multifocal and geographic retinal dysplasia in the dog—In vivo retinal micro-anatomy analyses. *Vet Ophthalmol.* 2020;23:292-304.
15. Mowat FM, Gervais KJ, Occelli LM, et al. Early-onset progressive degeneration of the area centralis in RPE65-deficient dogs. *Invest Ophthalmol Vis Sci.* 2017;58:3268-3277.
16. Minella AL, Occelli LM, Narfstrom K, et al. Central retinal preservation in rdAc cats. *Vet Ophthalmol.* 2017;21:224-232.
17. Osinchuk SC, Leis ML, Salpeter EM, Sandmeyer LS, Grahn BH. Evaluation of retinal morphology of canine sudden acquired retinal degeneration syndrome using optical coherence tomography and fluorescein angiography. *Vet Ophthalmol.* 2019;22:398-406.
18. Komaromy AM, Bras D, Esson DW, et al. The future of canine glaucoma therapy. *Vet Ophthalmol.* 2019;22:726-740.
19. Snyder KC, Oikawa K, Williams J, et al. Imaging distal aqueous outflow pathways in a spontaneous model of congenital glaucoma. *Transl Vis Sci Technol.* 2019;8:22.
20. Kuehn MH, Lipsett KA, Menotti-Raymond M, et al. A mutation in LTBP2 causes congenital glaucoma in domestic cats (*Felis catus*). *PLoS One.* 2016;11:e0154412.
21. Graham KL, McCowan CI, Caruso K, et al. Optical coherence tomography of the retina, nerve fiber layer, and optic nerve head in dogs with glaucoma. *Vet Ophthalmol.* 2019;23:97-112.
22. Soukup P, Maloca P, Altmann B, Festag M, Atzpodien EA, Pot S. Interspecies variation of outer retina and choriocapillaris imaged with optical coherence tomography. *Invest Ophthalmol Vis Sci.* 2019;60:3332-3342.
23. Jonnal RS, Kocaoglu OP, Zawadzki RJ, Lee SH, Werner JS, Miller DT. The cellular origins of the outer retinal bands in optical coherence tomography images. *Invest Ophthalmol Vis Sci.* 2014;55:7904-7918.
24. Spaide RF, Curcio CA. Anatomical correlates to the bands seen in the outer retina by optical coherence tomography: literature review and model. *Retina.* 2011;31:1609-1619.
25. Cuenca N, Ortuño-Lizarán I, Pinilla I. Cellular characterization of OCT and outer retinal bands using specific immunohistochemistry markers and clinical implications. *Ophthalmology.* 2018;125:407-422.
26. Spaide RF. Outer retinal bands. *Invest Ophthalmol Vis Sci.* 2015;56:2505-2506.
27. Spaide RF. Questioning optical coherence tomography. *Ophthalmology.* 2012;119:2203-2204.
28. Curcio CA, Sparrow JR, Bonilha VL, Pollreisz A, Lujan BJ. Re: Cuenca et al.: Cellular characterization of OCT and outer retinal bands using specific immunohistochemistry markers and clinical implications. *Ophthalmology.* 2018;125:407-422.
29. Staurengi G, Sadda S, Chakravarthy U, Spaide RF. International Nomenclature for Optical Coherence Tomography (INOCT) Panel. Proposed lexicon for anatomic landmarks in normal posterior segment spectral-domain optical coherence tomography: the IN*OCT consensus. *Ophthalmology.* 2014;121:1572-1578.
30. DeRamus ML, Stacks DA, Zhang Y, et al. GARP2 accelerates retinal degeneration in rod cGMP-gated cation channel beta-subunit knockout mice. *Sci Rep.* 2017;7:42545.
31. Beltran WA, Cideciyan AV, Guzewicz KE, et al. Canine retina has a primate fovea-like bouquet of cone photoreceptors which is affected by inherited macular degenerations. *PLoS One.* 2014;9:e90390.
32. Dufour VL, Yu Y, Pan W, Ying GS, Aguirre GD, Beltran WA. In vivo longitudinal changes in thickness of the canine postnatal retina. *Exp Eye Res.* 2020;192:107926.
33. Ofri R, Ekesten B. Baseline retinal OCT measurements in normal female beagles: the effects of eccentricity, meridian, and age on retinal layer thickness. *Vet Ophthalmol.* 2019;23:52-60.
34. Guzewicz KE, Cideciyan AV, Beltran WA, et al. BEST1 gene therapy corrects a diffuse retina-wide microdetachment modulated by light exposure. *Proc Natl Acad Sci USA.* 2018;115:E2839-E2848.
35. Espinheira Gomes F, Parry S, Ledbetter E. Spectral domain optical coherence tomography evaluation of the feline optic nerve and peripapillary retina. *Vet Ophthalmol.* 2019;22:623-632.
36. Ollivier FJ, Samuelson DA, Brooks DE, Lewis PA, Kallberg ME, Komaromy AM. Comparative morphology of the tapetum lucidum (among selected species). *Vet Ophthalmol.* 2004;7:11-22.
37. Gelatt KN, Gilger BC, Kern TJ. *Veterinary Ophthalmology: Two Volume Set.* Wiley; 2013.
38. Yamaue Y, Hosaka YZ, Uehara M. Spatial relationships among the cellular tapetum, visual streak and rod density in dogs. *J Vet Med Sci.* 2015;77:175-179.
39. Mowat FM, Petersen-Jones SM, Williamson H, et al. Topographical characterization of cone photoreceptors and the area centralis of the canine retina. *Mol Vis.* 2008;14:2518-2527.
40. Peichl L. Topography of ganglion cells in the dog and wolf retina. *J Comp Neurol.* 1992;324:603-620.
41. Garcia-Layana A, Cabrera-Lopez F, Garcia-Arumi J, et al. Early and intermediate age-related macular degeneration: update and clinical review. *Clin Interv Aging.* 2017;12:1579-1587.
42. Iwabe S, Ying GS, Aguirre GD, Beltran WA. Assessment of visual function and retinal structure following acute light exposure in the light sensitive T4R rhodopsin mutant dog. *Exp Eye Res.* 2016;146:341-353.
43. Palko JR, Iwabe S, Pan X, Agarwal G, Komáromy AM, Liu J. Biomechanical properties and correlation with collagen solubility profile in the posterior sclera of canine eyes with an ADAMTS10 mutation. *Invest Ophthalmol Vis Sci.* 2013;54:2685-2695.
44. Kundel HL, Polansky M. Measurement of observer agreement. *Radiology.* 2003;228:303-308.
45. Landis JR, Koch GG. The measurement of observer agreement for categorical data. *Biometrics.* 1977;33:159-174.

46. Marmor MF, Choi SS, Zawadzki RJ, Werner JS. Visual insignificance of the foveal pit: reassessment of foveal hypoplasia as fovea plana. *Arch Ophthalmol*. 2008;126:907-913.
47. Carpenter CL, Kim AY, Kashani AH. Normative retinal thicknesses in common animal models of eye disease using spectral domain optical coherence tomography. *Adv Exp Med Biol*. 2018;1074:157-166.
48. Dufour VL, Yu Y, Pan W, Ying GS, Aguirre GD, Beltran WA. In-vivo longitudinal changes in thickness of the postnatal canine retina. *Exp Eye Res*. 2020;192:107926.
49. Dysli C, Enzmann V, Sznitman R, Zinkernagel MS. Quantitative analysis of mouse retinal layers using automated segmentation of spectral domain optical coherence tomography images. *Transl Vis Sci Technol*. 2015;4:9.
50. Lozano DC, Twa MD. Quantitative evaluation of factors influencing the repeatability of SD-OCT thickness measurements in the rat. *Invest Ophthalmol Vis Sci*. 2012;53:8378-8385.
51. Srinivasan PP, Heflin SJ, Izatt JA, Arshavsky VY, Farsiu S. Automatic segmentation of up to ten layer boundaries in SD-OCT images of the mouse retina with and without missing layers due to pathology. *Biomed Opt Express*. 2014;5:348-365.
52. Hong EH, Ryu SJ, Kang MH, et al. Comparison of repeatability of swept-source and spectral-domain optical coherence tomography for measuring inner retinal thickness in retinal disease. *PLoS One*. 2019;14:e0210729.
53. Lee HJ, Kim MS, Jo YJ, et al. Ganglion cell-inner plexiform layer thickness in retinal diseases: repeatability study of spectral-domain optical coherence tomography. *Am J Ophthalmol*. 2015;160:283-289. e281.
54. Lee HJ, Kim MS, Jo YJ, Kim JY. Thickness of the macula, retinal nerve fiber layer, and ganglion cell layer in the epiretinal membrane: the repeatability study of optical coherence tomography. *Invest Ophthalmol Vis Sci*. 2015;56:4554-4559.
55. Kafieh R, Rabbani H, Abramoff MD, Sonka M. Intra-retinal layer segmentation of 3D optical coherence tomography using coarse grained diffusion map. *Med Image Anal*. 2013;17:907-928.
56. Kafieh R, Rabbani H, Kermani S. A review of algorithms for segmentation of optical coherence tomography from retina. *J Med Signals Sens*. 2013;3:45-60.
57. Chiu SJ, Allingham MJ, Mettu PS, Cousins SW, Izatt JA, Farsiu S. Kernel regression based segmentation of optical coherence tomography images with diabetic macular edema. *Biomed Opt Express*. 2015;6:1172-1194.
58. Lu S, Cheung CY, Liu J, Lim JH, Leung CKS, Wong TY. Automated layer segmentation of optical coherence tomography images. *IEEE Trans Biomed Eng*. 2010;57:2605-2608.
59. Syc SB, Saidha S, Newsome SD, et al. Optical coherence tomography segmentation reveals ganglion cell layer pathology after optic neuritis. *Brain*. 2012;135:521-533.
60. Zheng Y, Xiao R, Wang Y, Gee JC. A generative model for OCT retinal layer segmentation by integrating graph-based multi-surface searching and image registration. *Med Image Comput Comput Assist Interv*. 2013;16:428-435.
61. He YF, Sun YK & Chen M et al. Automatic segmentation of canine retinal OCT using adaptive gradient enhancement and region growing. *Medical Imaging 2016-Biomedical Applications in Molecular, Structural, and Functional Imaging* 9788, 2016.
62. Hogan D, Williams RW. Analysis of the retinas and optic nerves of achiasmatic Belgian sheepdogs. *J Comp Neurol*. 1995;352:367-380.
63. Hebel R. Distribution of retinal ganglion cells in five mammalian species (pig, sheep, ox, horse, dog). *Anat Embryol (Berl)*. 1976;150:45-51.

SUPPORTING INFORMATION

Additional supporting information may be found in the online version of the article at the publisher's website.

How to cite this article: Mischi E, Soukup P, Harman CD, et al. Outer retinal thickness and visibility of the choriocapillaris in four distinct retinal regions imaged with spectral domain optical coherence tomography in dogs and cats. *Vet Ophthalmol*. 2022;25(Suppl. 1):122-135. doi: [10.1111/vop.12989](https://doi.org/10.1111/vop.12989)